However, it is unknown whether TLR9 senses self-DNA to modulate CNS function in the absence of pathogen-derived DNA. In the present study, we have suggested that TLR9 senses self-DNA from degenerating hippocampal neurons to attenuate seizure-induced aberrant neurogenesis, revealing a role for TLR9 in maintaining brain integrity. TLR7-KO mice, in contrast, displayed no impaired phenotype, at least in neurogenesis. Moreover, when we pretreated CM from KA-treated neurons with RNase to deplete TLR7 ligand (RNA), the CM-induced elevation of *Tnf-α* expression in primary microglia was not abolished (Supplementary Fig. 14). These data suggest that self-RNA from degenerating neurons does not function as a TLR7 ligand for the regulation of neurogenesis following seizure, although TLR7 is known to recognize self-RNA and microRNA[31,32]. The microRNA let-7, a highly abundant regulator of gene expression in the CNS, activates TLR7 in neurons and induces neurodegeneration[31]. Neuronal TLR7 is also reported to sense self-RNA derived from neighbouring cells and thus to impair axonal outgrowth of cortical neurons[32]. These observations warrant further experimentation using TLR7-KO and/or a double-KO with TLR9 to gain a better understanding of how immune receptors recognize endogenous ligands from neighbouring CNS cells and modulate brain functions.

We have shown that the activation of TLR9 signalling in microglia induces TNF-α expression, resulting in the attenuation of aberrant neurogenesis in the hippocampus. Consistent with our findings, it has been reported that TNF receptor 1 (TNFR1) expressed in aNS/PCs is a negative regulator for adult hippocampal neurogenesis[23]. The loss of TNFR1 enhances seizure-mediated aNS/PC proliferation and increases neurogenesis in the hippocampus. TNF-α is a key factor in the immune response[33], but it is unclear whether TNF-α has any positive effects in the CNS since many studies have focused on its roles as a negative effector in neurodegenerative disorders such as Alzheimer's disease[34]. Thus, our results unveil a positive aspect of TNF-α function in the CNS for the maintenance of homoeostatic neurogenesis.

The findings that microglia are in close proximity to aNS/PCs (Supplementary Fig. 1a–c) and that inhibition of microglial activation after seizure exacerbates aberrant neurogenesis (Fig. 3e–h and Supplementary Fig. 2) highlight the importance of microglia for the regulation of adult neurogenesis in the aNS/PC niche. Consistent with these observations, several previous studies have suggested that microglia inhibit adult hippocampal neurogenesis[12,13]. However, it has also been suggested that activated microglia promote neurogenesis by secreting trypsinogen[35]. These contradictory assertions are probably due to the contribution of different subtypes of activated microglia to the regulation of neurogenesis. Microglia can undergo different modes of polarized activation, which give rise to potentially neurotoxic classic-M1 (characterized by the release of pro-inflammatory factors) or potentially neuroprotective alternative-M2 (characterized by the expression of anti-inflammatory cytokines) subtypes[10,36,37]. In the CNS, increasing evidence indicates that M1 microglia exacerbate neurodegenerative disease through the production of pro-inflammatory cytokines[10]. Minocycline is known as an inhibitor of M1 microglial activation since it selectively inhibits M1 microglia-related gene expression[21]. Therefore, it is plausible that M1 microglia release TNF-α and consequently attenuate seizure-induced aberrant neurogenesis.

In this study, we have identified a novel, intrinsic mechanism to attenuate aberrant neurogenesis that involves interactions between TLR9-expressing immune cells and neural cells. We show that TLR9 signalling activated by DNA from degenerating neurons induces TNF-α production in microglia, resulting in the inhibition of seizure-induced aberrant neurogenesis (Supplementary Fig. 15). Thus, microglia in the aNS/PC niche respond via TLR9 to the insult induced by seizure and ensure homoeostatic neurogenesis. However, we suspect that our proposed mechanism is one among many that contribute to homoeostatic neurogenesis, because the aNS/PC niche is composed of many types of cells and is vulnerable to a variety of pathological stimuli. Future studies will reveal as-yet-unknown mechanisms by which the niche reacts to these stimuli to ensure the maintenance of brain homoeostasis. Boosting the functions of these intrinsic mechanisms should offer therapeutic strategies for diseases associated with abnormal neurogenesis, such as major depression, ischaemia, Alzheimer's disease and epilepsy.

Methods

Animals. All efforts were made to minimize animal suffering and to reduce the number of animals used. Animals were housed on a 12/12-h light/dark cycle and fed *ad libitum*. TLR7-KO and TLR9-KO mice were on a C57BL/6 background. Sox2–GFP mice[38] were a gift from F.H. Gage (Salk Institute, USA). Male 8-week-old mice were used for this study. To induce seizure, the mice received i.p. injections of KA (30 mg kg^{-1}; Enzo Life Sciences) dissolved in saline. Behaviour of KA-treated mice was observed for 1 h after the injection and the seizure score was recorded, according to previously described criteria[39,40]. Briefly, we used the following seizure scale: no response (0), staring and reduced locomotion (1), activation of extensors and rigidity (2), repetitive head and limb movements (3), sustained rearing with clonus (4), loss of posture (5), and status epilepticus and death (6). The scores did not differ between WT and TLR9 KO mice following KA injection. To assess recurrent seizure severity, all mice were re-injected with KA (10 mg kg^{-1}) at 48 days after the first KA injection (30 mg kg^{-1}).

The day after KA injection, BrdU (50 mg kg^{-1}; Sigma) dissolved in saline was injected intraperitoneally into TLR7-KO, TLR9-KO and WT mice daily for 1 week to monitor cell proliferation, differentiation and survival. These mice were killed 1 day or 21 days after the last injection of BrdU. The day before seizure induction, minocycline (20 mg kg^{-1}; Sigma) dissolved in saline was injected intraperitoneally into TLR9-KO and WT mice once daily for 8 consecutive days to inhibit microglial activation. To inhibit seizure-induced TNF-α production, thalidomide (250 mg kg^{-1}; Sigma) dissolved in 0.5% carboxymethylcellulose (Sigma) was injected intraperitoneally into WT mice with the same time course as minocycline. For the inhibition of TLR9-dependent TNF-α production, mice were treated with thalidomide on day 1 after seizure and again the following day. To evaluate cell proliferation at each day, we injected BrdU into mice every 4 h (four times) at 1, 2, 3 and 4 days after KA administration and killed the mice 12 h after the last BrdU injection.

For the hippocampus-dependent recognition test, mice were transferred to the testing room and acclimated for at least 1 h before habituation and testing. Each mouse was habituated to the empty testing chamber (10 min) for 3 days after being handled for 3 days. The testing chamber was an opaque plastic chamber (50 × 50 × 30 cm). Two identical objects were placed in the testing chamber, and the mouse was allowed to explore the objects for 5 min as the training phase and then the mouse was taken out from the chamber. We then placed one of the two objects in a new position where is a diagonal corners with the object placed in familiar position (Fig. 5a). After a 5-min delay, the mouse was replaced in the testing chamber again. The mouse was given 5 min to explore the familiar and displaced objects during the testing phase. Behaviour was recorded with a video tracking system. Frequency of object interactions and time spent exploring each object were recorded for subsequent data analysis. The testing chamber and used objects were washed with 70% ethanol before the next mouse was tested. All mice were subjected to behavioural testing at 6 weeks after seizure.

All mice were treated according to Fundamental Guidelines for Proper Conduct of Animal Experiment and Related Activities in Academic Research Institutions under the jurisdiction of the Ministry of Education, Culture, Sports, Science and Technology of Japan.

Gene expression analysis. Total RNA was isolated from tissues and cells using Sepasol-RNA I Super G (Nacalai Tesque) following the manufacturer's instructions. RNA quality of all samples was checked by spectrophotometer. Reverse transcription reactions were carried out using the SuperScript VILO cDNA Synthesis Kit (Life Technologies) according to the kit protocol. Primer sequences used in this study can be found in Supplementary Table 1. qRT–PCR was performed with SYBR green fluorescent dye using Step One Plus (Applied Biosytems) and Mx3000 (Stratagene). GAPDH was used as an endogenous control to normalize samples.

Immunohistochemistry. We performed immunohistochemistry as described previously[41]. Briefly, male adult mouse brains were fixed in 4% paraformaldehyde and 40-μm sections were cut with a cryostat. For staining with anti-BrdU antibody,

brain sections were incubated for 15 min with 2 N HCl. The antibodies used were anti-BrdU (1:1,000, AbD Serotec), anti-DCX (1:500, Abcam), anti-CD68 (1:500, AbD Serotec), anti-Iba1 (1:500, Wako), anti-TLR9 (1:100, Imgenex), anti-GFAP (1:2,000, Millipore), anti-S100β (1:500, Sigma), anti-GFP (1:500, Aves Labs) and anti-NeuN (1:500, Millipore). Nuclei were stained using bisbenzimide H33258 fluorochrome trihydrochloride (Hoechst) (Nacalai Tesque).

Immunocytochemistry. Cells were fixed in 4% paraformaldehyde and processed for immunostaining as described[41]. Cells were stained with one of the following antibodies: anti-Iba1 (1:500, Abcam), anti-GFAP (1:500, Millipore), anti-active caspase3 (1:500, R&D Systems), anti-BrdU (1:500, AbD Serotec), anti-p65 (1:500, Abcam) and anti-CD11b (1:500, AbD Serotec). For anti-BrdU staining, fixed cells were incubated with 2 N HCl for 5 min. EdU staining was performed using the Click-iT EdU Alexa Fluor 555 Imaging Kit (Life Technologies) according to the supplier's protocol. Stained cells were visualized with a fluorescence microscope (Zeiss Axiovert 200M, Zeiss).

Confocal imaging. Fluorescence images were obtained on a confocal laser microscope (LSM710 and LSM780, Zeiss). For quantification of the percentage of NS/PCs contacted by microglia, Z-series stacks of confocal images of GFP-expressing Sox2-positive cells and Iba1-positive cells were taken. At least 50 randomly chosen GFP-positive cells in the DG per animal were analyzed. GFP-positive cells whose cell bodies contacted microglial processes or cell bodies were counted. For analysis of neuronal localization in the DG at 8 days after seizure, Z-series stacks of confocal images of DCX-positive cells with Hoechst staining were taken to determine the localization of DCX-positive cells. For analysis of dendritic complexity and measurement of dendrite length *in vivo*, three-dimensional reconstructions of the entire dendritic processes of individual DCX-positive neurons were made from Z-series stacks of confocal images as previously described[42]. Briefly, images were acquired at 0.5-μm intervals. The projection images were traced and analyzed with ImageJ. At least 10 randomly chosen DCX-positive cells in the DG per animal were analyzed. Sholl analysis for dendritic complexity was performed by counting the number of dendrites that crossed a series of concentric circles at 10-μm intervals from the cell soma.

Cell counts. BrdU-positive cells within the DG were counted using every 6th section (240 μm apart). The number of counted cells was then multiplied by six to provide an accurate estimation of the number of cells per DG. To calculate the total number of marker-double-positive cells, at least 200 randomly chosen BrdU-positive cells per animal were analyzed. Microscopic analysis yielded a ratio of BrdU-positive cells colabelled with DCX, NeuN, GFAP and S100β. These ratios were multiplied by the total number of BrdU-labelled cells to give estimates of the total number of BrdU-positive immature or mature neurons and BrdU-positive astrocytes. To estimate the ratio of surviving cells after seizure, the total number of BrdU-positive cells at 3 weeks post injection of BrdU was divided by the total number of BrdU-positive cells at day 1 post injection of BrdU.

Cell culture. We obtained primary microglia and astrocytes from mouse at postnatal day 1 (P1) using a previously described protocol[43], with some modifications. To obtain mixed glial cell cultures, cortexes of WT and TLR9-KO mice were carefully dissected after stripping of meninges. The tissue was digested with papain (Sigma) at 37 °C for 20 min. After centrifugation (200*g*, 5 min), the cell pellet was resuspended in alpha-Minimum Essential Medium (MEM) with 5% foetal bovine serum (FBS) and 0.6% glucose, and the suspension was passed through a 40-μm Cell Strainer (BD Falcon). After centrifugation (200*g*, 5 min), the cell pellet was resuspended in DMEM containing 10% FBS and a low concentration of GM-SCF (0.1 ng ml^{-1}; PeproTech) to enhance microglial proliferation. These mixed glial cells were plated in poly-L-lysine-coated T75 tissue culture flasks. The medium was renewed every 2–3 days. Ten days after plating, microglia and oligodendrocyte precursor cells (OPCs) were detached from astrocyte monolayer sheets by shaking, collected and plated onto uncoated 35-mm culture dishes to remove OPCs. After a 30-min incubation, the medium was removed by suction and DMEM containing 10% FBS without GM-SCF was added to the dish. Two days after plating, primary microglia from WT and TLR9-KO mice were used for assays.

After the shake-off procedure for the isolation of microglia, Trypsin EDTA solution (Nacalai Tesque) was added to the flask to obtain the remaining astrocytes, which were transferred to a 35-mm culture dish and maintained in DMEM containing 10% FBS. Two days after plating, the astrocytes were used for assays.

Neuronal cultures were prepared from P1 mouse hippocampus according to a previously described protocol[44], with some modification. In brief, the hippocampus was digested with papain at 37 °C for 20 min and triturated with a 1-ml pipette. MEM with 5% FBS and 0.6% glucose was added and the mixture was plated onto a poly-L-lysine-coated 35-mm culture dish. After 3 h, the medium was replaced with maintenance medium (Neurobasal Medium (Gibco) supplemented with B27 (Gibco)) containing cytosine β-D-arabinofuranoside (5 μM; Sigma) to eliminate proliferating cells. To avoid neuronal cell death by a complete medium change, half of the medium was replaced every 3 days with fresh maintenance medium. After 12 days, the neurons were used for assays.

To obtain NS/PCs, P1 mouse hippocampus was dissected and triturated in Hank's balanced salt solution. After centrifugation (200*g*, 5 min), the cell pellet was resuspended in N2-supplemented DMEM/F-12 medium containing 10 ng ml^{-1} bFGF (PeproTech), plated on a poly-L-ornithine/fibronectin-coated dish and incubated for 4 days. The cells were passaged by replating on an ornithine/fibronectin-coated dish in N2 medium with 10 ng ml^{-1} each of bFGF and EGF (PeproTech)[45]. NS/PCs that had been passaged 10 times were used for qRT–PCR analysis.

aNS/PC proliferation assay. For the *in vitro* aNS/PC proliferation assay, we used aNS/PCs derived from rat hippocampus as previously described[46]. To determine the effect of candidate cytokines, aNS/PCs were cultured in the presence of murine TNF-α, murine IL-12 and murine IFN-γ (all PeproTech) for 3 days. N2-supplemented DMEM/F-12 medium containing bFGF (5 ng ml^{-1}) was used as culture medium in this assay.

Cell supernatant collection. To analyze the role of microglia in aNS/PC proliferation, microglia obtained from WT mice were cultured in the presence or absence of ODN1585 (0.3 μM; InvivoGen), ODN1826 (1 μM; InvivoGen) and ODN2395 (1 μM; InvivoGen) for 3 h and washed with PBS. DMEM containing 10% FBS was added to microglial cultures and incubated for 21 h. CM was then collected. aNS/PCs were cultured with 30% microglial CM for 3 days. For the aNS/PC proliferation assay, either BrdU or EdU was added (to 10 μM) to the culture medium 30 min before fixation. For TNF-α neutralization experiments, microglial CM was supplemented with 10 μg ml^{-1} anti- mouse TNF-α (R&D Systems) or 10 μg ml^{-1} normal goat IgG as a control and incubated at 37 °C for 1 h before it was added to the aNS/PC culture.

To confirm microglial activation by endogenous ligand derived from neurons, neurons were cultured in the presence or absence of KA (100 μM) for 1 h and washed with Neurobasal Medium. To avoid neuronal cell death caused by a complete medium change, we then added a 1:1 mixture of fresh and used maintenance medium, which is CM from cultured neurons without any stimulation. After 24 h, we collected the CM. Primary microglia were treated with 30% neuronal CM. To determine whether endogenous ligand derived from degenerating neurons was DNA, CM from KA-treated neurons was pre-incubated with 50 μg ml^{-1} of DNase (Roche) at 37 °C for 1 h. For NF-κB activation analysis, primary microglia were treated with 30% CM from unstimulated or KA-stimulated neurons. Microglia cultured with the CM were stained with anti-p65 antibody. The TLR9 agonist ODN1826 was added to primary microglia as a positive control to induce the translocation of p65 protein into the nucleus. To determine whether NF-κB is activated by TLR9 signalling, microglia were pretreated with TLR9 antagonist (ODN2088) for 1 h before addition of CM and the translocation of p65 into the nucleus was examined.

Osmotic pump infusion. In murine TNF-α-infusion experiments, KA-treated TLR9-KO mice were infused with recombinant TNF-α (120 ng per day; PeproTech) into the right ventricle by osmotic minipumps (Alzet) for 5 days with the following coordinates: posterior = 0.34 mm from Bregma, lateral = 1 mm, ventral = 3 mm, as previously described[47].

Evans blue injection. A 2% solution of Evans blue dye (Sigma) in 0.9% NaCl was intravenously injected into WT and TLR9-KO mice in a dose of 2 ml kg^{-1} at 3 days after seizure. All mice were killed 3 h after the Evans blue injection.

Statistical analysis. Statistical comparisons were made by Student's *t*-test (for two-group comparisons) and analysis of variance (for multiple group comparisons) with Tukey *post-hoc* tests. Data represent mean + s.e.m.

References

1. Aimone, J. B., Deng, W. & Gage, F. H. Adult neurogenesis: integrating theories and separating functions. *Trends Cogn. Sci.* **14,** 325–337 (2010).
2. Ming, G. L. & Song, H. Adult neurogenesis in the mammalian brain: significant answers and significant questions. *Neuron* **70,** 687–702 (2011).
3. Parent, J. M. *et al.* Dentate granule cell neurogenesis is increased by seizures and contributes to aberrant network reorganization in the adult rat hippocampus. *J. Neurosci.* **17,** 3727–3738 (1997).
4. Lugert, S. *et al.* Quiescent and active hippocampal neural stem cells with distinct morphologies respond selectively to physiological and pathological stimuli and aging. *Cell Stem Cell* **6,** 445–456 (2010).
5. Okamoto, M. *et al.* Reduction in paracrine Wnt3 factors during aging causes impaired adult neurogenesis. *FASEB J.* **25,** 3570–3582 (2011).
6. Snyder, J. S., Soumier, A., Brewer, M., Pickel, J. & Cameron, H. A. Adult hippocampal neurogenesis buffers stress responses and depressive behaviour. *Nature* **476,** 458–461 (2011).
7. Song, J. *et al.* Neuronal circuitry mechanism regulating adult quiescent neural stem-cell fate decision. *Nature* **489,** 150–154 (2012).

8. Tremblay, M. E. *et al.* The role of microglia in the healthy brain. *J. Neurosci.* **31,** 16064–16069 (2011).
9. Nimmerjahn, A., Kirchhoff, F. & Helmchen, F. Resting microglial cells are highly dynamic surveillants of brain parenchyma *in vivo*. *Science* **308,** 1314–1318 (2005).
10. Saijo, K. & Glass, C. K. Microglial cell origin and phenotypes in health and disease. *Nat. Rev. Immunol.* **11,** 775–787 (2011).
11. Sierra, A. *et al.* Microglia shape adult hippocampal neurogenesis through apoptosis-coupled phagocytosis. *Cell Stem Cell* **7,** 483–495 (2010).
12. Gebara, E., Sultan, S., Kocher-Braissant, J. & Toni, N. Adult hippocampal neurogenesis inversely correlates with microglia in conditions of voluntary running and aging. *Front. Neurosci.* **7,** 145 (2013).
13. Sultan, S., Gebara, E. & Toni, N. Doxycycline increases neurogenesis and reduces microglia in the adult hippocampus. *Front. Neurosci.* **7,** 131 (2013).
14. Kawai, T. & Akira, S. The role of pattern-recognition receptors in innate immunity: update on Toll-like receptors. *Nat. Immunol.* **11,** 373–384 (2010).
15. Maroso, M. *et al.* Toll-like receptor 4 and high-mobility group box-1 are involved in ictogenesis and can be targeted to reduce seizures. *Nat. Med.* **16,** 413–419 (2010).
16. Laird, M. D. *et al.* High mobility group box protein-1 promotes cerebral edema after traumatic brain injury via activation of toll-like receptor 4. *Glia* **62,** 26–38 (2014).
17. Rolls, A. *et al.* Toll-like receptors modulate adult hippocampal neurogenesis. *Nat. Cell Biol.* **9,** 1081–1088 (2007).
18. Jessberger, S. *et al.* Epigenetic modulation of seizure-induced neurogenesis and cognitive decline. *J. Neurosci.* **27,** 5967–5975 (2007).
19. Kron, M. M., Zhang, H. & Parent, J. M. The developmental stage of dentate granule cells dictates their contribution to seizure-induced plasticity. *J. Neurosci.* **30,** 2051–2059 (2010).
20. Avignone, E., Ulmann, L., Levavasseur, F., Rassendren, F. & Audinat, E. Status epilepticus induces a particular microglial activation state characterized by enhanced purinergic signaling. *J. Neurosci.* **28,** 9133–9144 (2008).
21. Kobayashi, K. *et al.* Minocycline selectively inhibits M1 polarization of microglia. *Cell Death Dis.* **4,** e525 (2013).
22. Vallieres, L., Campbell, I. L., Gage, F. H. & Sawchenko, P. E. Reduced hippocampal neurogenesis in adult transgenic mice with chronic astrocytic production of interleukin-6. *J. Neurosci.* **22,** 486–492 (2002).
23. Iosif, R. E. *et al.* Tumor necrosis factor receptor 1 is a negative regulator of progenitor proliferation in adult hippocampal neurogenesis. *J. Neurosci.* **26,** 9703–9712 (2006).
24. Goshen, I. *et al.* Brain interleukin-1 mediates chronic stress-induced depression in mice via adrenocortical activation and hippocampal neurogenesis suppression. *Mol. Psychiatry* **13,** 717–728 (2008).
25. Han, X. *et al.* Forebrain engraftment by human glial progenitor cells enhances synaptic plasticity and learning in adult mice. *Cell Stem Cell* **12,** 342–353 (2013).
26. Koyama, R. *et al.* GABAergic excitation after febrile seizures induces ectopic granule cells and adult epilepsy. *Nat. Med.* **18,** 1271–1278 (2012).
27. Zhang, Q. *et al.* Circulating mitochondrial DAMPs cause inflammatory responses to injury. *Nature* **464,** 104–107 (2010).
28. Kawai, T. & Akira, S. Signaling to NF-κB by Toll-like receptors. *Trends Mol. Med.* **13,** 460–469 (2007).
29. Hemmi, H. *et al.* A Toll-like receptor recognizes bacterial DNA. *Nature* **408,** 740–745 (2000).
30. Oka, T. *et al.* Mitochondrial DNA that escapes from autophagy causes inflammation and heart failure. *Nature* **485,** 251–255 (2012).
31. Lehmann, S. M. *et al.* An unconventional role for miRNA: let-7 activates Toll-like receptor 7 and causes neurodegeneration. *Nat. Neurosci.* **15,** 827–835 (2012).
32. Liu, H. Y. *et al.* TLR7 negatively regulates dendrite outgrowth through the Myd88-c-Fos-IL-6 pathway. *J. Neurosci.* **33,** 11479–11493 (2013).
33. Trevejo, J. M. *et al.* TNF-α-dependent maturation of local dendritic cells is critical for activating the adaptive immune response to virus infection. *Proc. Natl Acad. Sci. USA* **98,** 12162–12167 (2001).
34. McCoy, M. K. & Tansey, M. G. TNF signaling inhibition in the CNS: implications for normal brain function and neurodegenerative disease. *J. Neuroinflammation* **5,** 45 (2008).
35. Nikolakopoulou, A. M., Dutta, R., Chen, Z., Miller, R. H. & Trapp, B. D. Activated microglia enhance neurogenesis via trypsinogen secretion. *Proc. Natl Acad. Sci. USA* **110,** 8714–8719 (2013).
36. Edwards, J. P., Zhang, X., Frauwirth, K. A. & Mosser, D. M. Biochemical and functional characterization of three activated macrophage populations. *J. Leukoc. Biol.* **80,** 1298–1307 (2006).
37. Miron, V. E. *et al.* M2 microglia and macrophages drive oligodendrocyte differentiation during CNS remyelination. *Nat. Neurosci.* **16,** 1211–1218 (2013).
38. D'Amour, K. A. & Gage, F. H. Genetic and functional differences between multipotent neural and pluripotent embryonic stem cells. *Proc. Natl Acad. Sci. USA* **100**(Suppl 1): 11866–11872 (2003).
39. Ziemann, A. E. *et al.* Seizure termination by acidosis depends on ASIC1a. *Nat. Neurosci.* **11,** 816–822 (2008).
40. Racine, R. J. Modification of seizure activity by electrical stimulation. II. Motor seizure. *Electroencephalogr. Clin. Neurophysiol.* **32,** 281–294 (1972).
41. Namihira, M. *et al.* Committed neuronal precursors confer astrocytic potential on residual neural precursor cells. *Dev. Cell* **16,** 245–255 (2009).
42. He, Y. *et al.* ALK5-dependent TGF-β signaling is a major determinant of late-stage adult neurogenesis. *Nat. Neurosci.* **17,** 943–952 (2014).
43. Giulian, D. & Baker, T. J. Characterization of ameboid microglia isolated from developing mammalian brain. *J. Neurosci.* **6,** 2163–2178 (1986).
44. Bekkers, J. M. & Stevens, C. F. Excitatory and inhibitory autaptic currents in isolated hippocampal neurons maintained in cell culture. *Proc. Natl Acad. Sci. USA* **88,** 7834–7838 (1991).
45. Abematsu, M. *et al.* Neurons derived from transplanted neural stem cells restore disrupted neuronal circuitry in a mouse model of spinal cord injury. *J. Clin. Invest.* **120,** 3255–3266 (2010).
46. Hsieh, J., Nakashima, K., Kuwabara, T., Mejia, E. & Gage, F. H. Histone deacetylase inhibition-mediated neuronal differentiation of multipotent adult neural progenitor cells. *Proc. Natl Acad. Sci. USA* **101,** 16659–16664 (2004).
47. Jang, M. H. *et al.* Secreted frizzled-related protein 3 regulates activity-dependent adult hippocampal neurogenesis. *Cell Stem Cell* **12,** 215–223 (2013).

Acknowledgements

We thank M. Yoshioka, I. Kirikae, J. Kohyama, N. Uezono, K. Ito, H. Tamura, S. Komai, S. Katada, T. Imamura and M. Namihira for experimental help and valuable comments. This work was funded by the Asahi Glass Foundation and a Grant-in-Aid for Exploratory Research from the Ministry of Education, Culture, Sports, Science and Technology of Japan (no. 24650198) and Core Research for Evolutional Science and Technology (CREST) from Japan Science and Technology Agency. T.M. received funding from a Sasakawa Scientific Research Grant and a Grant-in-Aid for JSPS Fellows (no. 13J09007).

Author contributions

T.M. contributed to the concept, design, execution and analysis of the experiments, provided funding and wrote the manuscript. N.M. contributed to the design and analysis of the experiments. Y.K. and B.J. contributed to analysis of the experiments. J.K., S.A. and T.K. provided advice and technical expertise. K.N. supervised the project and contributed to the concept and design of the experiments, provided funding and wrote the manuscript.

Additional information

Supplementary Information accompanies this paper at http://www.nature.com/naturecommunications

Competing financial interests: The authors declare no competing financial interest.

Reprints and permission information is available online at http://npg.nature.com/reprintsandpermissions/

How to cite this article: Matsuda, T. *et al.* TLR9 signalling in microglia attenuates seizure-induced aberrant neurogenesis in the adult hippocampus. *Nat. Commun.* 6:6514 doi: 10.1038/ncomms7514 (2015).

© 2015. Published by The Company of Biologists Ltd | Development (2015) 142, 910-920 doi:10.1242/dev.116996

RESEARCH ARTICLE

Gene activation-associated long noncoding RNAs function in mouse preimplantation development

Nobuhiko Hamazaki[1,2], Masahiro Uesaka[1,2], Kinichi Nakashima[2], Kiyokazu Agata[1] and Takuya Imamura[1,2,*]

ABSTRACT

In mice, zygotic activation occurs for a wide variety of genes, mainly at the 2-cell stage. Long noncoding RNAs (lncRNAs) are increasingly being recognized as modulators of gene expression. In this study, directional RNA-seq of MII oocytes and 2-cell embryos identified more than 1000 divergently transcribed lncRNA/mRNA gene pairs. Expression of these bidirectional promoter-associated noncoding RNAs (pancRNAs) was strongly associated with the upregulation of their cognate genes. Conversely, knockdown of three abundant pancRNAs led to reduced mRNA expression, accompanied by sustained DNA methylation even in the presence of enzymes responsible for DNA demethylation. In particular, microinjection of siRNA against the abundant pancRNA partner of interleukin 17d (*Il17d*) mRNA at the 1-cell stage caused embryonic lethality, which was rescued by supplying IL17D protein *in vitro* at the 4-cell stage. Thus, this novel class of lncRNAs can modulate the transcription machinery in *cis* to activate zygotic genes and is important for preimplantation development.

KEY WORDS: Long noncoding RNA, DNA demethylation, Early mouse preimplantation development, Zygotic gene activation, Epigenetic regulation, Pluripotency

INTRODUCTION

Transcription of the zygote genome begins mainly at the 2-cell stage. Genome-wide gene activation in the zygote, termed zygotic gene activation (ZGA), is regarded as crucial for embryos to acquire the potency to form all cell types. In the mouse, ZGA starts around the pronuclear stage, followed by a major wave of transcription at the 2-cell stage (Aoki et al., 1997; Latham et al., 1991). During ZGA, the patterns of various types of DNA and histone modification are dynamically reconstructed. For example, the sperm genome is tightly packaged by protamines that suppress nascent transcription (Braun, 2001). These sperm-derived protamines are replaced with maternally hyperacetylated histones that allow the onset of nascent transcription in the zygote (Santos et al., 2005). DNA demethylation is another well-known epigenetic event involved in the reconstruction of zygote chromatin structure. It has long been believed that after fertilization the bulk of the DNA, including repeat sequences such as long interspersed nuclear elements (LINEs), becomes demethylated as a major part of epigenetic reprogramming (Farthing et al., 2008; Mayer et al., 2000; Oswald et al., 2000). In actuality, DNA methylation at individual promoter regions differs during the epigenetic reprogramming (Borgel et al., 2010; Smallwood et al., 2011; Smith et al., 2012). The DNA methylation pattern of promoter regions seems to be determined in a gene-specific manner by an equilibrium between DNA methylation and demethylation. Thus, distinct and sequence-specific machineries should regulate this limited program of gene activation. One key issue is how such sequence-specific gene activation is achieved towards the acquisition of pluripotency in early mouse embryos.

Long noncoding RNAs (lncRNAs) constitute one group of factors that can explain such local epigenetic alterations. The number of known lncRNAs is now rapidly increasing, and experimental evidence for epigenetic alterations mediated by long intergenic noncoding RNAs, a fraction of lncRNAs, is accumulating. For example, *HOTAIR* acts as a chromatin repressor at hundreds of promoters with polycomb repressive complex 2 (Gupta et al., 2010; Rinn et al., 2007; Tsai et al., 2010). Another set of lncRNAs transcribed from bidirectional promoters, named promoter-associated noncoding RNAs (pancRNAs), are poly(A)$^+$ RNAs involved in the sequence-specific upregulation of their oppositely transcribed partner genes (Imamura et al., 2004b; Tomikawa et al., 2011). Some of these poly(A)$^+$ RNAs have been confirmed to induce DNA demethylation in their promoter regions in a sequence-specific manner (Tomikawa et al., 2011). We and another group have also reported that thousands of pancRNAs are generated by transcription of the antisense strand and exhibit expression changes coordinated with their cognate gene. Moreover, pancRNA possesses the potential to enhance partner gene expression in a tissue-specific manner in mouse and chimpanzee brain and heart (Uesaka et al., 2014) and during embryonic stem cell (ESC) differentiation (Sigova et al., 2013).

Now, the directional RNA-seq technique has become powerful enough to be applied to very early stage embryos to see whether RNA-directed gene activation occurs in a significant fraction of genes, not only for cell differentiation but also for the acquisition of pluripotency. Therefore, we have started to analyze such comprehensive data to test the idea that the onset of pancRNA expression at ZGA can also activate partner gene expression in a gene-specific manner. In this study, to identify divergently transcribed pancRNA/gene pairs, we obtained the transcriptome of mouse oocytes and showed that more than 1000 such pairs are expressed at ZGA. By manipulating the abundant transcriptional machineries that involve pancRNA, we showed that pancRNAs are functionally associated with the activation of their partner genes. One such pancRNA for the expression of *Il17d*, a member of the interleukin gene family, was shown to be indispensable for embryonic development.

[1]Department of Biophysics and Global COE Program, Graduate School of Science, Kyoto University, Kitashirakawa-Oiwake, Sakyo-ku, Kyoto 606-8502, Japan. [2]Division of Basic Stem Cell Biology, Department of Stem Cell Biology and Medicine, Graduate School of Medical Sciences, Kyushu University, 3-1-1 Maidashi, Higashi-ku, Fukuoka 812-8582, Japan.

*Author for correspondence (imamura@scb.med.kyushu-u.ac.jp)

Received 24 August 2014; Accepted 5 January 2015

Development (2015) 142, 910-920 doi:10.1242/dev.116996

RESULTS

The identification of more than 1000 antisense pancRNAs in mouse preimplantation embryos

To examine whether pancRNAs are induced after fertilization, we generated a total of 111 million directional RNA-seq reads using an Illumina HiSeq2000 from mouse metaphase II (MII) oocytes and 420 million directional RNA-seq reads from 2-cell embryos (see Materials and Methods). These reads were mapped to the mouse mm10 genome. Our RNA-seq data showed robust reproducibility among biological replicates (Pearson correlation coefficient, r>0.99; supplementary material Fig. S1). 5′-3′ mapping bias was comparable to that of RNA-seq data for oocytes in previous studies (Park et al., 2013) (supplementary material Fig. S2). In order to verify the strandedness of our directional RNA-seq data, we mapped the reads to known RefSeq genes and calculated the proportion that mapped on the correct strand. The results showed that 99.1% of the reads from MII oocytes and 96.9% of the reads from the fertilized 2-cell embryos mapped on the correct strand. Using our high-resolution datasets, we identified 618 and 1129 candidate pancRNAs in MII oocytes and 2-cell embryos, respectively (Fig. 1A).

Characterization of pancRNA-partnered genes

To test the hypothesis that pancRNAs contribute to the upregulation of their partner genes during ZGA, we examined the expression pattern of the pancRNAs and their mRNAs. We found that 836 of the 1129 pancRNAs were co-expressed with the corresponding mRNAs in 2-cell embryos (Fig. 1B). We further investigated

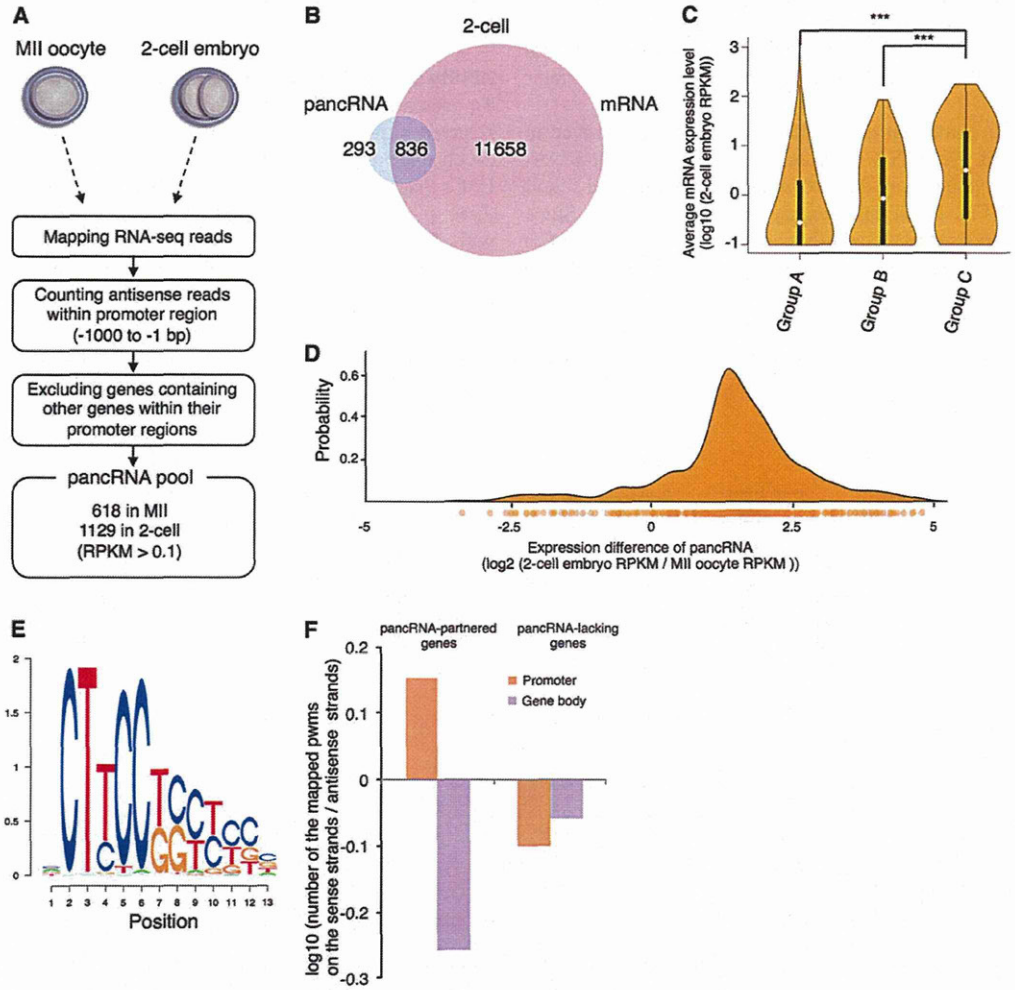

Fig. 1. Characterization of pancRNAs by directional RNA-seq. (A) Screening of pancRNA datasets. One hundred oocytes or 2-cell embryos were used for each analysis, and four replicates were made for the statistical tests. (B) Numbers of pancRNA and mRNA species present in 2-cell embryos. (C) Violin plot of mRNA levels of 2-cell embryo genes with and without pancRNAs. Groups A, B and C comprise mRNAs without pancRNAs (11658), with the 100 most weakly expressed pancRNAs, and with the 100 most strongly expressed pancRNAs, respectively. Violin width and white circles indicate gene density and median expression levels of mRNAs, respectively. Box plots were merged and are indicated by black bars. ***P<0.001. (D) Expression difference of the pancRNA partners of the upregulated genes and their probability visualized as a density plot. Twofold upregulated genes (which correspond to 520 of the 836 genes in B) were selected. Below the density plot is a unidimensional plot of the expression difference of each pancRNA (circles), in which density is expressed by color intensity. (E) A frequently observed sequence motif in the promoter regions of pancRNA-partnered genes. (F) The frequency of the sequence motif in various gene regions. Sequences with 90% or greater identity to the position weight matrix (pwm) of the motif shown in E were categorized according to their presence on the sense or antisense strand of the promoter (−500 to −1 bp) and gene body (+1 to +500 bp) regions. The TSSs of the pancRNA-partnered genes provide the switching points for the observed asymmetric distribution of the CT-rich sequence.

Development (2015) 142, 910-920 doi:10.1242/dev.116996

whether the pancRNA/mRNA pairs exhibit coordinated changes of expression, and found that most of the upregulated pancRNA/mRNA pairs showed coordinated upregulation in 2-cell embryos (supplementary material Fig. S3). As shown in Fig. 1C, we compared expression levels among three classes of genes that were expressed in 2-cell embryos: genes whose corresponding pancRNA is not transcribed (Group A), and those whose partner is among the 100 most weakly (Group B) or 100 most strongly (Group C) expressed of the 836 pancRNAs. The average gene expression level correlated with the presence of the respective pancRNA, and the expression levels of the Group C genes were significantly higher than those of Group A and B genes. Moreover, the difference in pancRNA expression level between MII and 2-cell embryos was positively correlated with that of the partner mRNA (Fig. 1D). Interestingly, based on the gene ontology function enrichment analysis, we found that cell death-related genes were enriched among co-upregulated pancRNA-partnered genes (supplementary material Tables S1 and S2). These results support our hypothesis that zygotic pancRNAs are involved in the upregulation of their cognate genes.

To test whether particular sequences are potentially involved in the regulation of pancRNA expression in zygotic pancRNA-partnered genes, we performed *de novo* motif searching and found a CT-rich motif (Fig. 1E; supplementary material Fig. S4A). Since pancRNA-partnered genes frequently contain a CpG island (CpGi) within their promoter region (supplementary material Fig. S4B), we investigated whether CT-rich motifs were enriched within the CpGi-type promoters. We calculated the CT-rich motif frequency within the promoters of CpGi-type and non-CpGi-type genes, and found that the CT-rich motif was present more frequently in the former (56.1% versus 44.8%; supplementary material Fig. S4C). These results suggest that the CT-rich motif is associated with CpGi. Most importantly, the distribution pattern of this CT-rich motif clearly differed between pancRNA-partnered genes and pancRNA-lacking genes (Fig. 1F). In pancRNA-partnered genes, the CT-rich motif was frequently observed on the sense strand of the promoter and on the antisense strand of the gene body. By contrast, in pancRNA-lacking genes, the CT-rich motif was observed on the antisense strand of not only the gene body but also the promoter (supplementary material Fig. S5). This indicates that the transcription start sites (TSSs) of the pancRNA-partnered genes are the switching points for the observed asymmetric distribution of the CT-rich motif.

Ability of pancRNAs to regulate gene activation

To examine the function of the ZGA-associated pancRNA, we selected highly expressed pancRNAs that were upregulated at the 2-cell stage and whose expression was maintained at a high level in ESCs (supplementary material Table S3), and characterized the three most highly expressed in ESCs, namely those partnered with *Il17d* (*pancIl17d*), *Mospd3* (*pancMospd3*) and *Tbc1d22a* (*pancTbc1d22a*) (Fig. 2A). First, we examined their expression

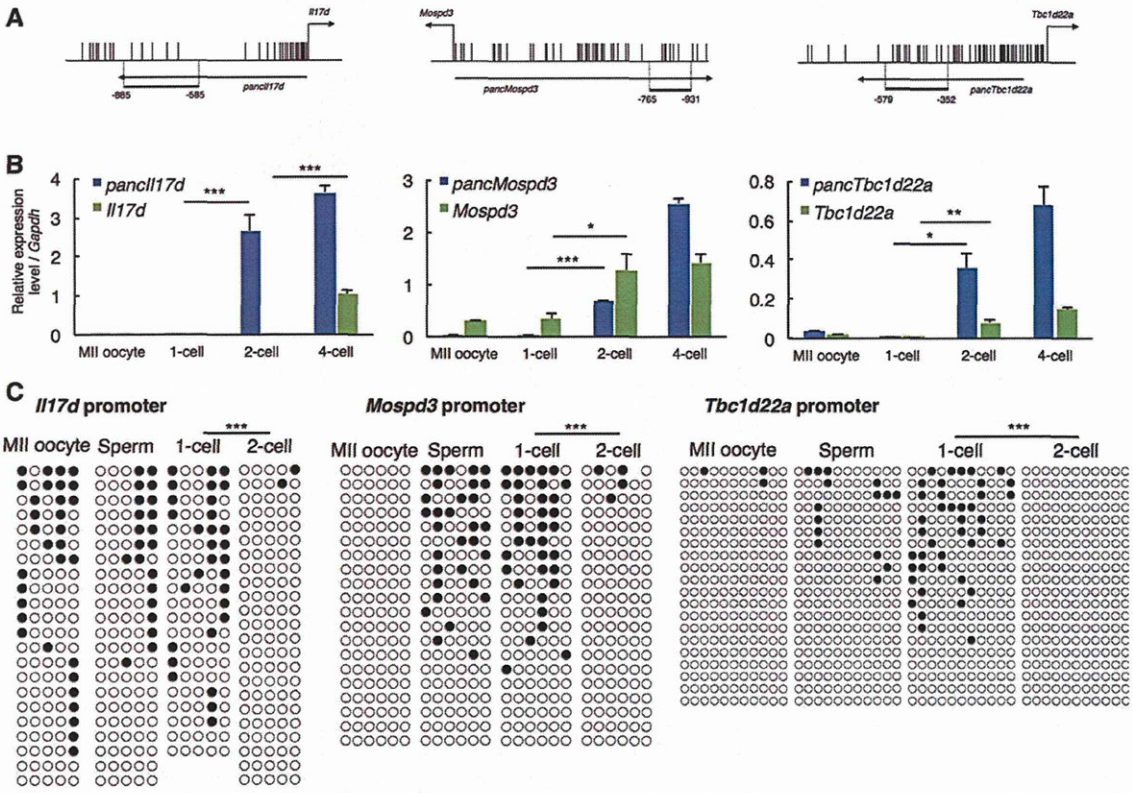

Fig. 2. Effect of pancRNA knockdown on the expression of the counterpart gene during early development. (A) 5′-regions of mouse *Il17d*, *Mospd3* and *Tbc1d22a*. Vertical lines mark the locations of CpG dinucleotides. Thick horizontal lines denote the regions analyzed by bisulfite sequencing. Primer positions are numbered relative to the TSS of each gene. (B) qPCR analysis of pancRNA and mRNA at the *Il17d*, *Mospd3* and *Tbc1d22a* loci in MII oocytes and in fertilized 1-cell, 2-cell and 4-cell embryos. Error bars indicate s.e.m. (C) DNA methylation levels of the promoter regions of *Il17d*, *Mospd3* and *Tbc1d22a* in MII oocytes, sperm and fertilized 1-cell and 2-cell embryos. Filled and open circles indicate methylated and unmethylated cytosines, respectively. **P*<0.05; ***P*<0.01; ****P*<0.001.

Development (2015) 142, 910-920 doi:10.1242/dev.116996

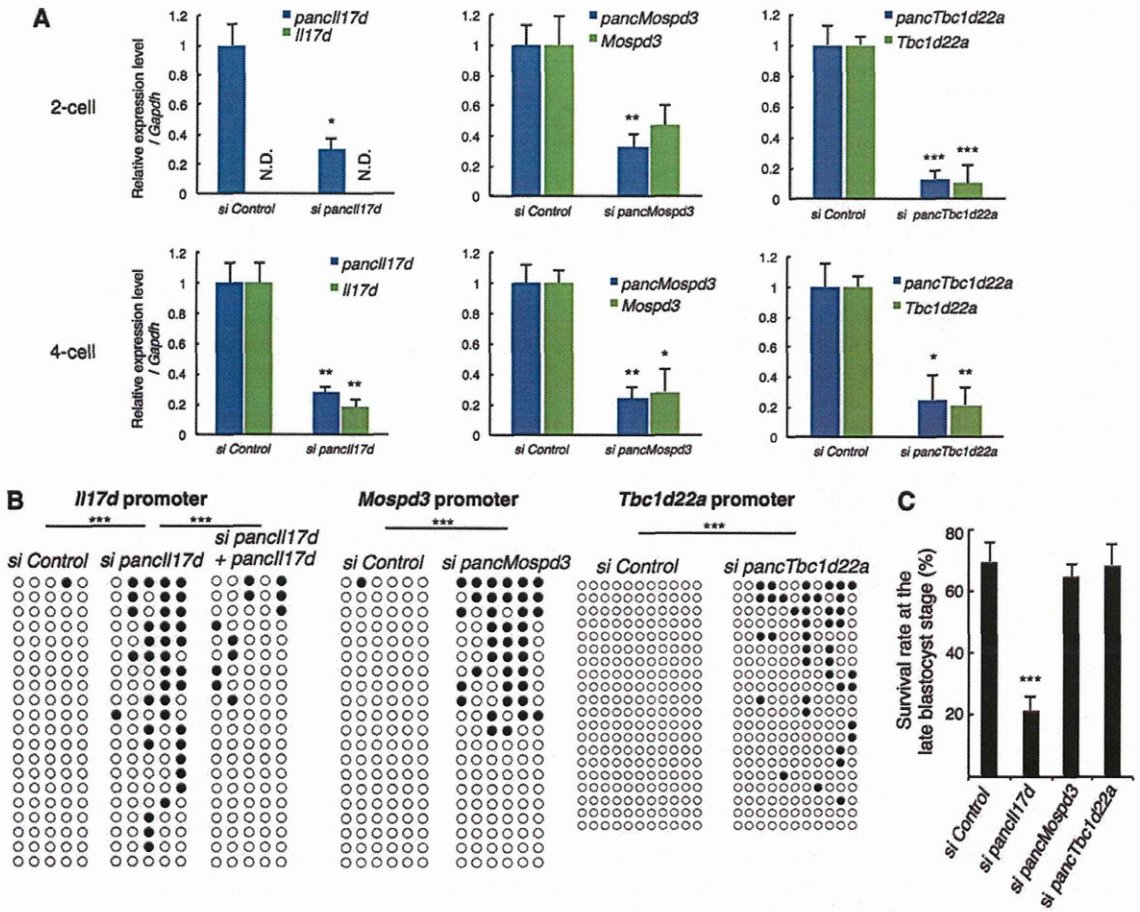

Fig. 3. Effect of knockdown of pancRNAs on partnered gene expression and on DNA methylation. (A) Expression levels of the indicated pancRNAs and their genes measured by qPCR in siRNA-injected 2-cell and 4-cell embryos. *Il17d* expression was not detectable (N.D.) in 2-cell embryos. (B) DNA methylation levels of the corresponding promoters in siRNA-injected embryos. The regions analyzed are displayed in Fig. 1A. (C) Effect of pancRNA knockdown on blastocyst formation. Asterisks indicate significant differences compared with si Control samples. The numbers of embryos used for injection of si Control, si *pancIl17d*, si *pancMospd3* and si *pancTbc1d22a* siRNAs were 261, 251, 78 and 70, respectively. *P<0.05; **P<0.01; ***P<0.001. Error bars indicate s.e.m.

patterns in the MII oocyte, sperm, and fertilized 1-cell and 2-cell embryo by RT-qPCR (Fig. 2B). We confirmed that all of these pancRNAs were expressed at the 2-cell stage, and found that the expression of *Mospd3* and *Tbc1d22a* mRNAs was also upregulated at the 2-cell stage (Fig. 2B, middle and right panels), whereas the expression of *Il17d* mRNA was first detected at the 4-cell stage (Fig. 2B, left panel). Thus, expression of the pancRNA preceded or occurred simultaneously with that of the mRNA at these loci during early embryogenesis.

Next, we analyzed whether the promoter methylation status reflects the gene activation/repression status. Since core promoter regions, which frequently show high CpG density, tend to be constitutively hypomethylated, and the flanking sequences with lower CpG density tend to be associated with developmental gene regulation (Meissner et al., 2008), we surveyed such developmentally regulated regions using publicly available MethylC-seq data of mouse germ cells and 2-cell embryos (Wang et al., 2014) at the three loci (supplementary material Fig. S6). Bisulfite sequencing indicated that this region in the *Il17d* promoter is considerably methylated at the MII oocyte, sperm and 1-cell stages (Fig. 2C). By contrast, this region became almost completely demethylated by the 2-cell stage, while the region located nearer the TSS was constitutively free of methylation, as expected from the MethylC-seq data (supplementary material Fig. S7). Similarly, the promoter regions of *Mospd3* and *Tbc1d22a* were methylated at the MII oocyte, sperm and 1-cell stages, and their DNA methylation levels decreased by the 2-cell stage. The concordance between the observed kinetics of expression of the pancRNAs and the changes in DNA demethylation raised the possibility that these pancRNAs mediate gene activation through epigenetic changes.

Since we previously found that pancRNAs could activate gene expression in rat differentiated cell lines (Tomikawa et al., 2011), we tested whether these developmentally expressed pancRNAs could be involved in the gene upregulation in early mouse embryos by knocking them down using siRNAs. We found that microinjection of siRNA for *pancIl17d*, *pancMospd3* or *pancTbc1d22a* into the pronucleus suppressed expression of the partner mRNA at the 2-cell and 4-cell stage, when partner expression normally begins (Fig. 3A), and this suppression was accompanied by a lack of decline in the methylation level in the respective promoter region (Fig. 3B; supplementary material Fig. S8). At the *Il17d* locus, this knockdown effect could be rescued by co-injection of the *pancIl17d* overexpression vector (Fig. 3B). Overexpressed *pancIl17d* might work as a sponge for the siRNA, and these pancRNAs might mediate acquisition of the hypomethylated status of the corresponding promoters and potentiate subsequent gene expression after fertilization.

Development (2015) 142, 910-920 doi:10.1242/dev.116996

Developmental defect caused by *pancIl17d* knockdown during preimplantation stages

To investigate the effects of knocking down the above three pancRNAs on preimplantation development, we monitored the rate of successful blastocyst formation in the knockdown embryos (Fig. 3C). 69.6±6.4% of control siRNA-injected, 64.8±4.0% of *pancMospd3* knockdown and 68.6±6.6% of *pancTbc1d22a* knockdown embryos successfully developed to the late blastocyst stage *in vitro*. By contrast, only 21.5±4.7% of *pancIl17d* knockdown embryos reached the late blastocyst stage (Fig. 3C). This developmental defect was also produced using another siRNA for *pancIl17d* (supplementary material Fig. S9). Regarding *pancMospd3* knockdown, although we could not see clear effects in the blastocysts, we found a deficiency of hatching after extending the culture of such embryos. After 5 days, a significant fraction of the *pancMospd3* knockdown embryos did not hatch from the zona pellucida, whereas most of the control embryos hatched (supplementary material Fig. S10A,B). Similar results were observed in ESCs: *pancMospd3* knockdown resulted in a decreased number of cells compared with the control ESCs (supplementary material Fig. S10C).

Since the effect of *pancIl17d* knockdown was drastic, we focused on investigating the roles of this pancRNA in embryonic development. Many *pancIl17d* knockdown embryos died between the 8-cell and early blastocyst stages. To establish whether cell death was enhanced in the *pancIl17d* knockdown embryos, we performed TdT-mediated dUTP nick-end labeling (TUNEL) staining of the *pancIl17d* knockdown embryos at the morula stage (Fig. 4A). Consistent with a previous report (Brison and Schultz, 1997), control embryos underwent little apoptosis during blastocyst formation. By contrast, *pancIl17d* knockdown embryos exhibited multiple TUNEL-positive blastomeres, suggesting that many *pancIl17d* knockdown embryos died by the blastocyst stage due to excessive apoptosis. It is noteworthy that the developmental capacity to form a blastocyst was restored when recombinant mouse IL17D protein (rIL17D) was added to the medium at the 4-cell stage, although the knockdown effect continued until the morula stage (Fig. 4B,C). The addition of rIL17D significantly increased the rate of success of blastocyst formation in *pancIl17d* knockdown embryos (from 21.5±2.7% to 62.1±5.9%; Fig. 4D). These results suggest that *pancIl17d* plays an important role in blastocyst formation by upregulating the partner gene.

In order to assess the role of *pancIl17d* in preimplantation embryos, we performed RNA-seq of *pancIl17d* knockdown morula embryos and compared the data with those for control siRNA-injected morula embryos (Fig. 4E). Gene ontology analysis revealed that apoptosis-related genes were enriched among the upregulated genes in the knockdown embryos (supplementary material Table S4). This is in accord with the observation that aberrant apoptosis is induced by *pancIl17d* knockdown, as shown in Fig. 4A. Interestingly, embryonic development-related genes were enriched among the downregulated genes. The second and third most highly expressed genes among the downregulated genes were *Nanog* and *Cdx2*, respectively, which encode transcription factors important for maintaining pluripotency and for the specification of cell lineages to generate trophectoderm, respectively (Chambers et al., 2003; Strumpf et al., 2005) (supplementary material Fig. S11). For example, the importance of pancRNAs for trophectoderm cell generation was supported by immunostaining of CDX2 of *pancIl17d* knockdown blastocysts, which showed that some outer blastomeres of *pancIl17d* knockdown embryos lost CDX2 expression (Fig. 4F). Therefore, *pancIl17d* seems important for the capacity to differentiate to generate trophectoderm cells.

Impairment of *in vitro* colony formation from *pancIl17d* knockdown embryos

To further investigate the significance of *pancIl17d* for embryonic development, we plated the surviving *pancIl17d* knockdown blastocysts in medium containing mouse LIF and inhibitors for MEK1/2 (MAP2K1/2) and GSK3β (2i medium), conditions that are frequently utilized for the culture of ground-state ESCs, and harvested the cultures after 10 days. Whereas about 70% of the control siRNA-injected embryos produced ESC-like colonies on average, only 10-20% of the *pancIl17d* knockdown embryos did so (Fig. 5A). Even when *pancIl17d* knockdown embryos did produce colonies, they were significantly smaller than those derived from control siRNA-injected embryos (Fig. 5B,C), indicating that *pancIl17d* knockdown decreases the ability to form a colony. These knockdown-induced impairments were also rescued by the addition of rIL17D to the culture medium at the 4-cell stage, strongly suggesting that the effects of *pancIl17d* knockdown are mediated by the downregulation of *Il17d* gene expression.

We further investigated the effect of *pancIl17d* knockdown in ESCs. siRNA-induced *pancIl17d* knockdown resulted in a decrease in the number of ESCs compared with the control siRNA (Fig. 5D). When *pancIl17d* was knocked down in ESCs, TUNEL-positive cells were significantly increased compared with the control (Fig. 5E). These results indicated that the loss of *pancIl17d* led to apoptotic cell death also in ESCs. In parallel, we analyzed the proliferative ability of the *pancIl17d* knockdown ESCs by performing a 5-ethyl-2′-deoxyuridine (EdU) incorporation experiment. The number of EdU-positive cells was significantly decreased in the *pancIl17d* knockdown cells compared with the control cells (Fig. 5F). These inhibitory effects of pancRNA knockdown on the proliferation of ESCs were reproduced by mRNA knockdown (Fig. 5D-F). Taken together, these results indicate that the *pancIl17d-Il17d* pair forms a molecular axis that is necessary for both cell survival and proliferation.

We analyzed the expression of pluripotency marker genes, including *Oct3/4* (*Pou5f1*), by RT-qPCR. Knockdown of *pancIl17d* or of *Il17d* mRNA caused significant decreases in the expression levels of *Oct3/4*, *Klf4*, *c-Myc* and *Cdh1*, but not of *Sox2* (Fig. 5G). We also performed the embryoid body (EB) formation assay using shRNA-transfected ESCs (supplementary material Fig. S12). EB size was altered by transfection of shRNA for *pancIl17d*, accompanied by increased expression levels of *Otx1* and *Gata6*, which are marker genes for the ectodermal and endodermal lineages, respectively. This indicated that *pancIl17d* knockdown causes abnormal EB formation.

Identification of the pathway triggering pancRNA-mediated gene upregulation

A previous study showed that base excision repair (BER) components, including poly(ADP-ribose) polymerase (PARP), contribute to DNA demethylation in preimplantation embryos (Hajkova et al., 2010). Therefore, we added a PARP inhibitor, 3-aminobenzamide (ABA), to the embryo culture medium to clarify whether promoter demethylation requires the BER pathway. The addition of ABA resulted in inhibition of DNA demethylation of the *Il17d* promoter region at the 2-cell stage (Fig. 6A; supplementary material Fig. S13), leading to downregulation of the partner mRNA (supplementary material Fig. S14). However, the addition of ABA did not change pancRNA expression, suggesting that expression of *pancIl17d* itself is regulated independently of the BER pathway and DNA methylation.

Development (2015) 142, 910-920 doi:10.1242/dev.116996

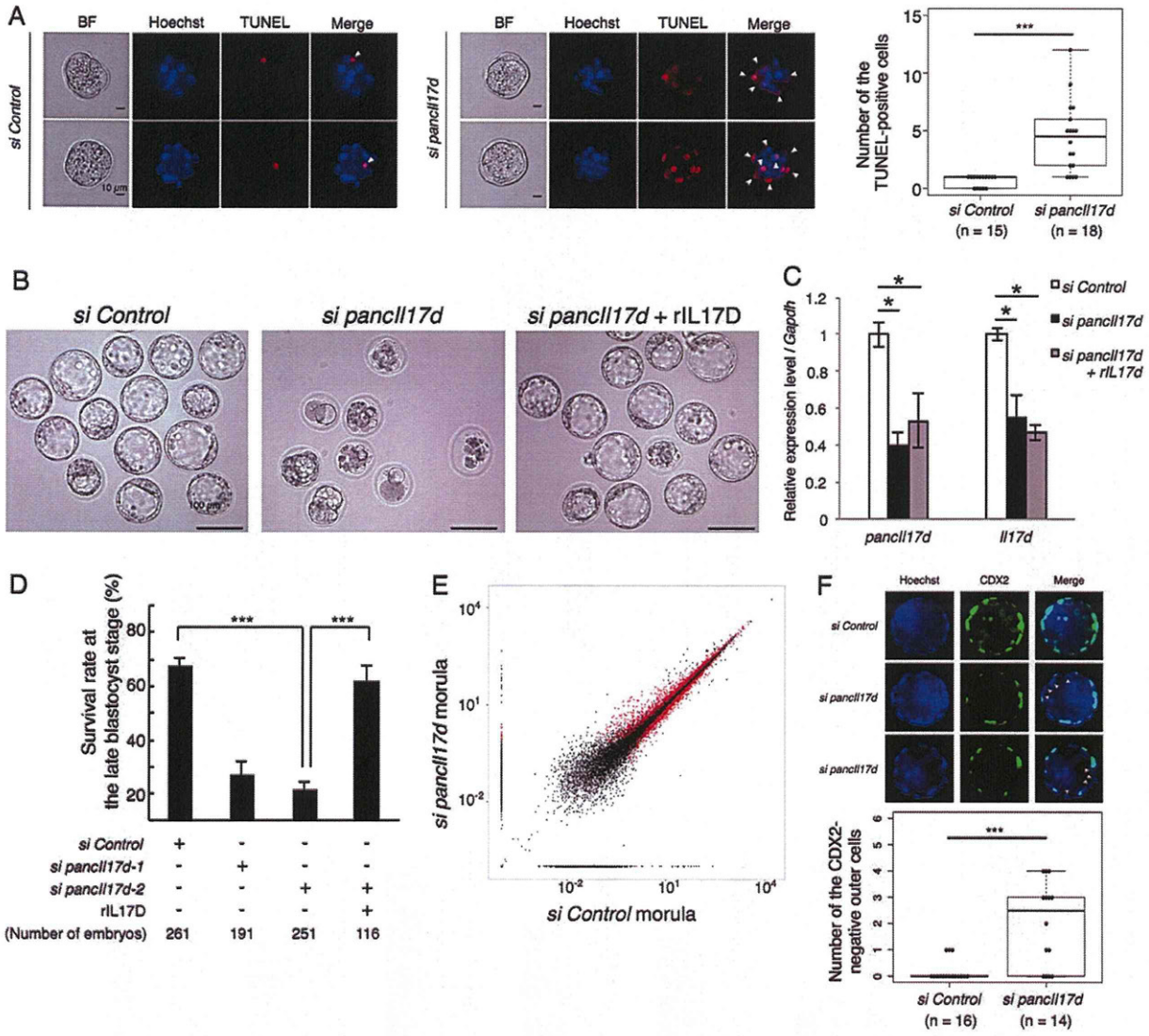

Fig. 4. Developmental defects induced by *pancII17d* knockdown and rescue by addition of recombinant IL17D protein. (A) TUNEL assay of morula embryos. Arrowheads indicate TUNEL-positive blastomeres. *pancII17d* knockdown embryos showed increased TUNEL-positive cells. Two representative blastomeres are shown. To the right is a box plot of the number of TUNEL-positive cells in each embryo. (B) Morphology of late blastocysts. (C) Expression levels of *pancII17d* and *Il17d* measured by qPCR in control, *pancII17d* knockdown and rIL17D-supplemented *pancII17d* knockdown morula embryos. (D) Survival rate of control and *pancII17d* knockdown embryos at day 4.5 of *in vitro* culture. Two different siRNAs targeting *pancII17d* were used. (E) Scatter plots of gene expression in control and *pancII17d* knockdown morula embryos based on the RPKMs of RefSeq genes. Red dots indicate the genes that show statistically significant changes. (F) Immunostaining of CDX2 protein in control and *pancII17d* knockdown late blastocyst. Arrowheads indicate CDX2-negative outer cells Beneath is a box plot of the number of CDX2-negative outer cells in each embryo **P*<0.05; ****P*<0.001. Error bars indicate s.e.m.

Considering recent reports showing that ten-eleven translocation (TET) enzymes are among the key molecules triggering BER pathways (Kohli and Zhang, 2013; Teperek-Tkacz et al., 2011), we knocked down *Tet3*, which is abundantly expressed in early embryos, and *Tet2*, which shows lower expression than *Tet3* in preimplantation embryos (supplementary material Table S5). *Tet3* knockdown embryos showed significantly higher DNA methylation levels than control embryos. By contrast, knockdown of *Tet2* did not induce significant DNA methylation changes (Fig. 6B), suggesting that *Tet3*, but not *Tet2*, is required for DNA demethylation at the *Il17d* promoter. Fig. 6C summarizes pancRNA-mediated sequence-specific gene upregulation.

DISCUSSION

The key molecules that enable sequence-specific gene activation to initiate embryonic development remain largely unknown. Here, we identified more than 1000 pancRNAs as candidates of such key molecules in early mouse embryos. To examine the function of the ZGA-associated pancRNA, we focused on three abundant pancRNAs: *pancII17d*, *pancMospd3* and *pancTbc1d22a*. We found that these three pancRNAs had the ability to reprogram the epigenetic status of promoter regions for gene activation in a sequence-specific manner. We also proved that *pancII17d* plays an essential role in early embryogenesis. Our study thus sheds light on novel mechanisms by which a fraction of zygotically activated

Development (2015) 142, 910-920 doi:10.1242/dev.116996

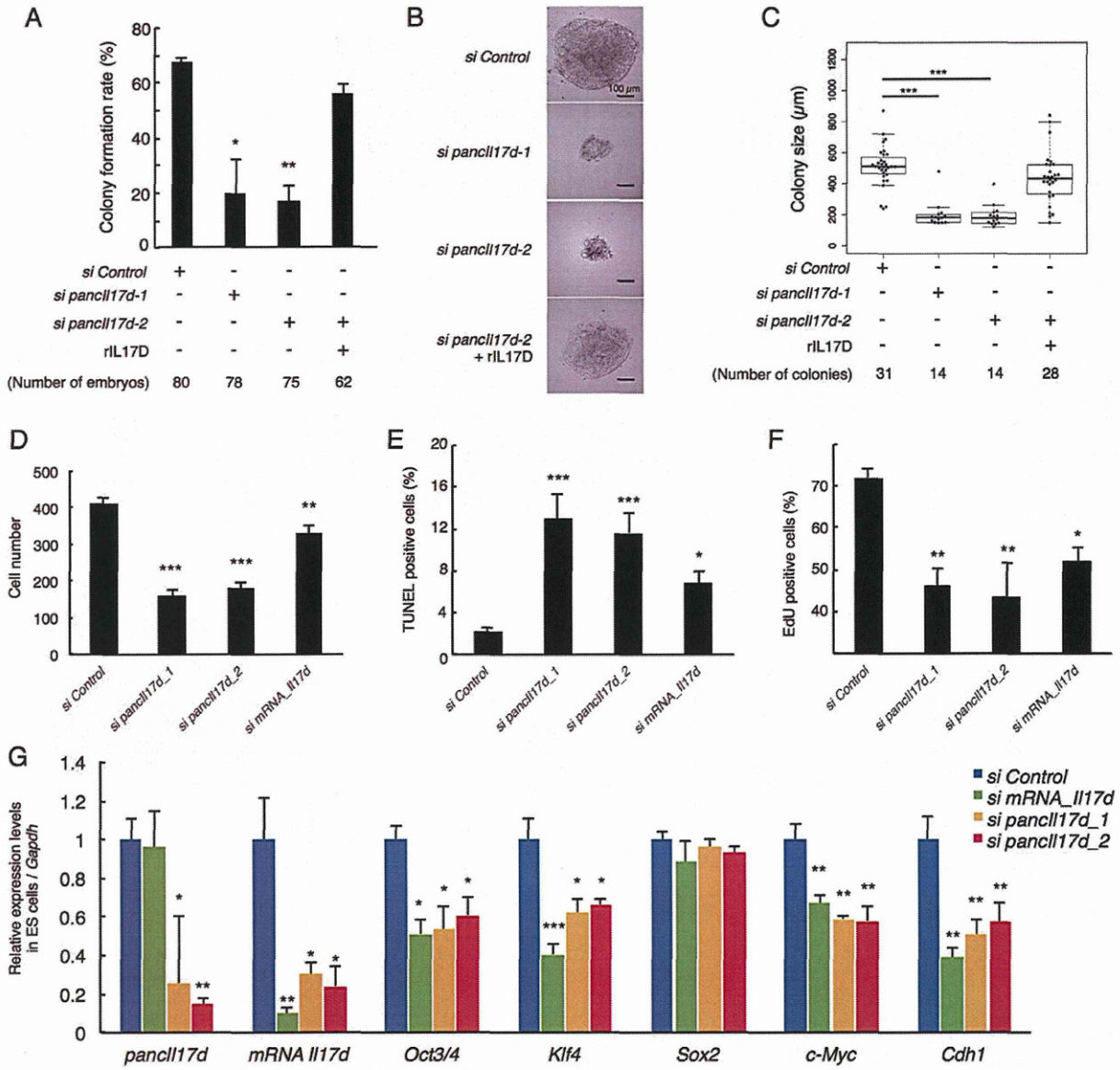

Fig. 5. Effect of *pancII17d* knockdown on colony outgrowth from blastocysts and on ESC properties. (A) Rate of colony outgrowth from knockdown and rescued blastocysts. Colonies growing after 10 days in culture were counted. (B) Representative images of colonies derived from siRNA-injected embryos. (C) Box plot of diameter of colonies derived from pancRNA knockdown blastocysts. (D) Number of ESCs 24 h after siRNA introduction by electroporation. (E) Proportion of apoptotic cells detected by TUNEL staining in knocked down ESCs after siRNA introduction. (F) Proportion of proliferating ESCs, as analyzed by EdU labeling. (G) Expression levels of *pancII17d*, *II17d* and pluripotency marker genes in ESCs, as detected by RT-qPCR. *Gapdh* was used as a control. The expression level in control-transfected ESCs was set as 1. Asterisks indicate significant differences compared with si Control samples. **P*<0.05; ***P*<0.01; ****P*<0.001. Error bars indicate s.e.m.

lncRNAs enhance partner gene promoter activity for subsequent mouse embryogenesis.

The effects of pancRNAs on gene regulation in many biological processes

In this study, the RNA-seq method was adapted for small-scale samples to yield RNA-seq data at a level comparable to that generated from large-scale samples (supplementary material Fig. S2). Indeed, pancRNAs were detected from more than 1000 promoter regions during ZGA (Fig. 1A). This is consistent with previous reports showing that thousands of pancRNAs are transcribed in terminally differentiated mouse tissues and ESCs (Sigova et al., 2013; Uesaka et al., 2014). Thus, a substantial number of pancRNAs seems to be expressed in various cell contexts, including totipotent stages, as we show here. Since pancRNAs and mRNAs exhibit coordinated expression changes not only in somatic cells but also in preimplantation embryos (Fig. 1D), pancRNAs might be commonly utilized for gene activation from the zygotic to the terminally differentiated stages. According to their partner genes, pancRNAs function in the regulation of many biological processes, a conclusion supported by our *pancII17d* knockdown experiments.